Available online at www.sciencedirect.com

ScienceDirect

Geochimica et Cosmochimica Acta 281 (2020) 102–117

Geochimica et Cosmochimica Acta

www.elsevier.com/locate/gca

Experimental constraints on magnesium isotope fractionation during abiogenic calcite precipitation at room temperature

Xin-Yang Chen [a,*], Fang-Zhen Teng [a], William R. Sanchez [b], Christopher S. Romanek [b,*], Antonio Sanchez-Navas [c], Mónica Sánchez-Román [d]

[a] *Isotope Laboratory, Department of Earth and Space Sciences, University of Washington, Seattle, WA, USA*
[b] *NASA Astrobiology Institute and Department of Earth and Environmental Sciences, Furman University, Greenville, SC, USA*
[c] *NASA Astrobiology Institute and Departamento de Mineralogía y Petrología-IACT, Universidad de Granada-CISC, 18071 Granada, Spain*
[d] *NASA Astrobiology Institute and Earth Sciences Department, Vrije Universiteit Amsterdam, de Boelelaan 1085, 1081 HV Amsterdam, the Netherlands*

Received 14 November 2019; accepted in revised form 29 April 2020; available online 11 May 2020

Abstract

Magnesium (Mg) isotopes in carbonate minerals are a useful proxy for paleoclimate studies, but interpretations are often limited by an inadequate understanding of the various factors controlling Mg isotopic fractionation during carbonate formation. Previous work has studied a number of parameters including aqueous chemistry, mineralogy, temperature, and precipitation rate. However, little is known about the impact of solid/solution ratio, calcite growth mechanism, and crystal morphology on isotope fractionation. In this work, two groups of seeded chemo-stat calcite precipitation experiments were conducted at 25 °C to explore the potential impact of crystal growth and morphology on the fractionation of Mg isotopes. Group-1 experiments (G1) contained nine individual runs that were performed under identical physicochemical conditions, except for solid/solution ratio and the length of an experiment. The isotope fractionation between precipitated calcite and aqueous solution is limited, with $\Delta^{26}Mg_{cal\text{-}sol}$ ranging from −2.58 to −2.40‰ and an average of -2.49 ± 0.12‰ (2SD, $n = 9$). The Group-2 experiments (G2) contained 3 paired runs with solution Mg/Ca molar ratios of 0.5, 2.0, and 5.0, and yielded $\Delta^{26}Mg_{cal\text{-}sol}$ values that ranged from −2.69 to −2.36‰ with an average of -2.62 ± 0.25‰ (2SD, $n = 6$).

The average $\Delta^{26}Mg_{cal\text{-}sol}$ value for both sets of experiments is -2.54 ± 0.22‰ (2SD, $n = 15$), and it is independent of precipitation rate, solution Mg/Ca molar ratio, solid/solution ratio, amount of overgrowth, and mol% Mg content in overgrowth. The form and texture of the calcite overgrowths in our experiments range from {104} rhombohedra with smooth crystal faces containing few macrosteps to {104} rhombohedra containing extensive evidence for 2-D nucleation on crystal faces, to more steeply sided rhombohedra {0*kl*}. While significant changes in crystal morphology are related to solid/solution ratio and solution composition in the G1 and G2 experiments, respectively, there was no difference in Mg isotope systematics, suggesting that crystal morphology does not affect the Mg isotopic composition of calcite within the range of features investigated and 2-D nucleation may be less affected by calcite growth kinetics than a spiral growth mechanism. Integrating our results with previous published values, an equilibrium isotopic fractionation factor of -2.47 ± 0.09‰ (weighted average ± weighted 2SD, $n = 70$) between calcite and aqueous solutions is derived at room temperature.

Keywords: Carbonate; Crystal morphology; Magnesium isotopes; Equilibrium isotope fractionation; Chemo-stat

* Corresponding authors.
E-mail addresses: xinychen@uw.edu (X.-Y. Chen), Christopher.romanek@furman.edu (C.S. Romanek).

https://doi.org/10.1016/j.gca.2020.04.033
0016-7037/

1. INTRODUCTION

Carbonates are important archives for a wide range of biological, geochemical, and sedimentological processes. Whether formed biogenically or abiogenically, calcite commonly contains magnesium (Mg) in various amounts when it precipitates from Mg-bearing aqueous solutions (Mucci and Morse, 1983; Mucci, 1987). The concentration of Mg in Mg-calcite is considered as a reliable proxy for the composition and temperature of paleoseawater (Morse et al., 1997; Elderfield and Ganssen, 2000). Studies on natural carbonate systems have reported a wide range of Mg isotopic compositions for speleothems (–4.47 to –1.69‰), deep sea and pelagic carbonates (–5.14 to –3.89‰) and documented a considerable Mg isotope fractionation between carbonate minerals and aqueous Mg (Galy et al., 2002; Buhl et al., 2007; Immenhauser et al., 2010; Riechelmann et al., 2012; Higgins and Schrag, 2010, 2012, 2015; Teng, 2017). In addition, previous investigations of marine biogenic carbonates have revealed significant Mg isotopic fractionations in skeletal carbonates (Chang et al., 2004; Pogge von Strandmann et al., 2014; Hippler et al., 2009; Ra et al., 2010; Wombacher et al., 2011; Saenger and Wang, 2014). These large Mg isotope variations were interpreted to reflect either kinetic or equilibrium fractionations, which were affected by various factors, such as the mineralogy of the precipitates, temperature, precipitation rate and biological effect.

Unequivocal interpretation of Δ^{26}Mg data from natural carbonates is limited by an incomplete understanding of the nature of fractionation mechanisms (i.e., equilibrium vs. kinetic) and other factors controlling Mg isotopic fractionation during calcite precipitation. A highly constrained isotope fractionation factor during abiotic calcite precipitation helps to understand the isotopic expressions of "vital effect" during biomineralization processes.

The abiogenic heterogeneous growth of calcite crystals typically involve several processes: (1) transport of ions from the aqueous solution to the mineral surface, (2) adsorption at the surface of the crystals, (3) diffusion at the surface of the crystal to the reactive site, and (4) a surface reaction that leads to bond formation and/or ion exchange with the solids (Morse et al., 1997; DePaolo, 2011). Magnesium isotopes may be fractionated during any of these processes. Experimental calibrations and theoretical calculations were conducted to provide a more thorough understanding of the various processes affecting the fractionation of Mg isotopes between aqueous Mg and associated precipitates (Kisakürek et al., 2009; Rustad et al., 2010; Li et al., 2012; Saulnier et al., 2012; Mavromatis et al., 2012, 2013, 2017a, 2017b; Wang et al., 2013, 2017, 2019; Pinilla et al., 2015; Gao et al., 2018). However, as the experimental conditions vary from one set to another, the observed range of Mg isotopic fractionations between calcite and aqueous solution ($\Delta^{26}Mg_{cal\text{-}sol}$) becomes difficult to explain. Moreover, theoretical calculations often predict a significantly larger magnitude of isotope fractionation than experimental observations (Rustad et al., 2010; Schauble, 2011; Pinilla et al., 2015; Schott et al., 2016; Wang et al., 2017, 2019; Gao et al., 2018).

Additionally, a recent study by Ning et al. (2019) on natural dolomite samples suggested that crystal morphologies probably do not affect their Mg isotopic compositions. But for calcite, it is unclear how crystal morphology and growth habit may impact Mg isotopic fractionation, much as it does for the bulk incorporation of Mg on different crystal surfaces (e.g., Davis et al., 2000, 2004; Paquette and Reeder, 1990, 1995; Wasylenki et al., 2005). The growth of calcite crystals is fundamentally controlled by microscopic step propagation, which can be influenced by solution saturation state (Teng et al., 2000). Atomic force microscopy (AFM) studies suggest that at lower degrees of calcite supersaturation ($\Omega < 2.2$), precipitation is dominated by spiral growth initiated by surface imperfections from screw dislocations. When $\Omega > 2.2$, direct nucleation on the surfaces as two dimensional (2-D) islands becomes increasingly important (Teng et al., 1999, 2000). The transition from spiral growth to 2-D nucleation has been shown to affect Ca isotope fractionation (Nielsen et al., 2012) and different growth mechanisms may have imposed different Mg isotopic fractionation during calcite precipitation.

In this study, 15 chemo-stat experiments were conducted at room temperature (~25 °C) to explore the impact of various solid/solution ratios and solution Mg/Ca ratios on calcite crystal morphology and their relationships with Mg isotope fractionation between calcite and solution. The results of this study provide a critical evaluation of calcite crystal morphology and $\Delta^{26}Mg_{cal\text{-}sol}$ during abiogenic precipitation. In conjunction with previous published work, we assess the equilibrium Mg isotope fractionation factor at room temperature.

2. MATERIALS AND METHODS

2.1. Reagents and experimental design

Inorganic calcite precipitation experiments were conducted using the chemo-stat approach to form Mg-bearing calcite from supersaturated solutions following methods modified from Romanek et al. (1992). The detailed experimental methods are reported in the Supplemental Material. Calcite precipitation reactions were performed in 1000 mL Schott Duran™ reaction vessels that contained a Teflon-coated magnetic stir bar and a pH electrode (Fig. 1). Titrants from distinct cation and anion titrant reservoirs were added to each vessel using a Cole-Parmer MasterFlex L/S™ peristaltic pump. All titrant and master solutions were prepared from 1 M stock solutions of $CaCl_2 \cdot 2H_2O$, $MgCl_2 \cdot 6H_2O$ (Fisher Certified ACS) and $NaHCO_3$ (ACROS Organics ACS) reagents.

Two sets of experiments were conducted using different types of calcite seed. The temperature of both sets of experiments was kept constant at 25 °C. The chemical composition of the reactive solutions remained relatively constant throughout the experiments. Group-1 (G1) experiments were designed to grow Mg-calcite under identical physicochemical conditions for various lengths of time and different solution to solid ratios using Mg-free seed crystals from J.T.Baker™ (Baker Analyzed™ reagent-grade $CaCO_3$, Lot H22339) with a BET measured specific surface area of

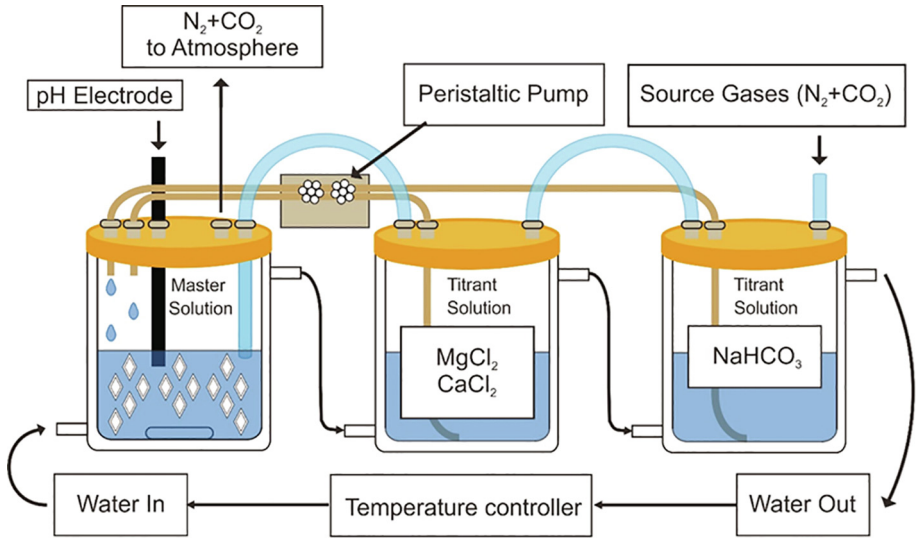

Fig. 1. Schematic of chemo-stat experimental setup. The master solution hosts magnesian calcite growth on calcite seed crystals. Titrant solutions of $CaCl_2$ and $MgCl_2$, and $NaHCO_3$ are transferred to the master solution by a peristaltic pump to replace ions removed from solution due to calcite precipitation. Experiments are conducted under a constant partial pressure of CO_2 to facilitate gas-solution exchange of aqueous and gaseous CO_2.

0.25 m^2 g^{-1} and contain less than 0.020% Mg. For the G1 experiments, approximately 50 mg of seed material was used in five experiments (RS7, 10, 17, 18, 23) yielding a solid/solution ratio of 10^2 mg L^{-1}, while two experiments (RS24, 25) used 500 mg of seed for a solid/solution ratio of 10^3 mg L^{-1}, and two final experiments (RS28, 29) used 5000 mg of seed for a solid/solution ratio of 10^4 mg L^{-1}. The pH values for the G1 solutions were ~7.0 and they were maintained at a constant partial pressure of CO_2 (pCO_2) of 5atm.%.

Group-2 (G2) experiments were conducted as pairs at aqueous Mg/Ca ratios of ~0.5 (FU12, 125), ~1.0 (FU60, 48), and ~5.0 (FU105, 98). The values for pCO_2 varied from 3 to 100 atm.%, which resulted in a wider range of pH values (6.4–7.8) than the G1 experiments. In the G2 experiments, a distinct reagent-grade calcite powder from ACROS Organics™ ($CaCO_3$, 99+%, Lot: A0350502) with a BET determined specific surface area of 0.78 m^2 g^{-1}, was used except for experiment FU125, which used the Mg-free seed. Notably, the ACROS seed contained an average of 1.61 ± 0.9 mol% Mg, which provided an opportunity to explore the potential pathway dependence of Mg calcite formation on a Mg-bearing solid surface. Both seed materials were 100% calcite with no detectable aragonite or vaterite.

2.2. Experimental procedure for calcite precipitation

Predetermined aliquots of $CaCl_2$ and $MgCl_2$ stock solution and de-ionized water (18.2 MΩ) were added to a reaction vessel to prepare a master solution of specified chemical composition. The solution was bubbled with pure $CO_{2(g)}$ to establish a pH of <4.0 before a predetermined aliquot of stock $NaHCO_3$ solution was added to the vessel to bring the total volume to 500 mL. Thereafter the concentration of CO_2 in the bubbling gas stream was adjusted using proportional flow controllers to a predetermined CO_2/N_2 ratio depending on the desired pCO_2 for each experiment, which ranged from 3 to 100 atm.%. Chemical equilibration of the fluid was achieved within 30 minutes with the stabilization of solution pH, at which time 25 mL aliquots of master solution were collected for alkalinity and cation analysis.

An experiment was initiated with the introduction of a predetermined mass of calcite seed (e.g., ~50 mg) to the master solution. The peristaltic pump was engaged, and titrants were introduced dropwise with no visible sign of spontaneous nucleation upon introduction into the master solution. Experiments were conducted over various lengths of time (45 min−98 h) depending on the mass of overgrowth desired or until the reaction vessel was filled. At the conclusion of an experiment, aliquots of master solution were collected again for cation and anion analysis. Solid samples were collected using a flask filtration apparatus containing a 0.45 μm polycarbonate filter (Millipore™). The stir bar, reaction vessel, bubbler and pH electrode were thoroughly rinsed and cleaned with methanol to ensure all solid carbonate was transferred to the filter. The filter was then transferred to a petri dish and covered to dry for 24 hours, after which it was reweighed to determine the mass of solid collected at the conclusion of an experiment.

2.3. Analytics

Alkalinity measurements were made using a Metrohm™ 905 Titrando, 800 Dosino, and 801 Stirrer apparatus. Autotitration measurements used certified NIST-traceable 0.1 M HCl titrant and pH buffers. Repeated measurement of in-house standards showed the precision of the analysis to be ±2%. An Orion 912600 combination pH electrode

calibrated with certified NIST traceable buffers was used to determine the solution pH. All solutions were analyzed for Mg and Ca concentration using a Liberty Series II inductively coupled plasma atomic emission spectroscopy (ICP-AES) (Varian) with a precision ~3% (RSD) based on repeated measurement of in-house standards. The mass of newly formed calcite overgrowth was determined by the mass difference between the final solid and the initial seed. Precipitation rate (mol m^{-2} s^{-1}) of calcite overgrowth was calculated by dividing the mass of the overgrowth by the molar weight of $CaCO_3$, the mass normalized surface area of the seed material and the length of an experiment. The mineralogy of the final solid was determined using a Rigaku Miniflex II X-ray diffractometer from 10° to 34.5° 2θ. The Mg concentration in the final solid was determined by ICP-AES with an estimated precision of 5%. The mole fraction of $MgCO_3$ in the overgrowth was calculated by dividing the molar Mg concentration of the final solid by the percentage of overgrowth. Calcite seed crystals and the final solid were examined by scanning electron microscope (SEM) to determine the crystal habit and morphology using a Carl Zeiss Auriga FE-SEM. The aqueous chemistry and calcite saturation state of the initial and final master solutions were modeled using PHREEQC software (Parkhurst and Appelo, 2013) and the phreeqc.dat database.

2.4. Magnesium isotope analysis

Magnesium isotopic ratios were analyzed at the Isotope Laboratory of the University of Washington following previously established protocols (Teng et al., 2007, 2015; Ling et al., 2013). Approximately 5–10 mg of pre-cleaned calcite precipitate was first dissolved in 0.6 M HCl at room temperature, dried down and subsequently re-dissolved in 12 M HCl. Similarly, around 300 μL of the initial and final reaction solutions were evaporated to dryness and re-dissolved in 12 M HCl. Separation of Mg from Ca was achieved by cation exchange chromatography using Bio-Rad 200–400 mesh AG50W-X12 resin and eluted with 12 M HCl. Magnesium was further purified using AG50W-X8 resin (200–400 mesh) and eluted with 1 M HNO_3. This second step was repeated for all samples to ensure complete separation of Mg from major matrix elements. Two internal standards (San Carlos olivine and Hawaiian seawater) were processed together with the samples during each batch of column chemistry.

Isotopic ratios were determined using the standard-sample bracketing method on a *Nu Plasma II* multi-collector inductively coupled plasma mass spectrometer in 3% HNO_3 solutions with the three Mg isotopes (^{24}Mg, ^{25}Mg, ^{26}Mg) simultaneously measured. The Mg concentration between the sample and the standard was matched within 5%. Magnesium isotopic values are reported in δ notation as per mil variations relative to the standard DSM3:

$$\delta^{x}\mathrm{Mg}(‰) = \left[\left({}^{x}\mathrm{Mg}/{}^{24}\mathrm{Mg}\right)_{\mathrm{sample}} / \left({}^{x}\mathrm{Mg}/{}^{24}\mathrm{Mg}\right)_{\mathrm{DSM3}} - 1\right] \times 1000 \quad (1)$$

where x refers to either mass 25 or 26. The $\delta^{26}Mg$ values for San Carlos olivine and Hawaiian seawater standards during the course of the study are $-0.26 \pm 0.06‰$ (2SD, n = 6), and $-0.86 \pm 0.06‰$ (2SD, n = 3), respectively, which are in agreement with published values (Teng et al., 2015; Hu et al., 2016).

The Mg isotope fractionation between Mg-calcite and reactive solution is expressed as:

$$\Delta^{26}\mathrm{Mg}_{\mathrm{cal\,-\,sol}} = \delta^{26}\mathrm{Mg}_{\mathrm{cal}} - \delta^{26}\mathrm{Mg}_{\mathrm{sol}} \approx 1000 \ln\left(\alpha^{26/24}_{\mathrm{cal\,-\,sol}}\right) \quad (2)$$

The uncertainty in Mg isotopic fractionation factor $\Delta^{26}Mg_{cal\text{-}sol}$ is calculated by error propagation:

$$\mathrm{SD}_{\Delta 26} = \sqrt{\mathrm{SD}^2_{\mathrm{cal}} + \mathrm{SD}^2_{\mathrm{sol}}} \quad (3)$$

where SD_{cal} and SD_{sol} are the standard deviations of measured $\delta^{26}Mg_{cal}$ and $\delta^{26}Mg_{sol}$, respectively.

3. RESULTS

Relevant experimental conditions and solution chemistry of individual runs are summarized in Table 1. The Mg isotopic compositions of master solutions before and after the precipitation experiments, as well as the final solids are reported in Table 2.

3.1. Chemical and isotopic composition of solutions

The Mg/Ca molar solution ratio of the G1 experiments was ~0.5, with average Ca and Mg concentrations of 12.15 ± 1.41 and 5.57 ± 0.33 mM, respectively. The average calcite saturation state (Ω) for each individual experiment ranged from 2.92 to 6.80 for the G1 experiments and 2.22 to 10.22 for the G2 experiments. The pH and pCO_2 of the G1 experiments were kept constant at ~6.9 and 5 atm.%, respectively. The average alkalinity of the G1 solutions was around 13.6 meq L^{-1} and slightly decreased to 11.8 meq L^{-1} after calcite precipitation. In comparison, the 6 runs of the G2 experiments were conducted under variable Mg/Ca molar solution ratios that ranged from 0.46 to 4.72. The average ionic strength of each individual experimental solution, as determined by the total dissolved constituents, was relatively low, ranging from 57 to 204 mM (Table 1). The calcite precipitation rate (Log R) displayed a relatively narrow range ($R = 10^{-5.65}$–$10^{-6.45}$ mol m^{-2} s^{-1}) for the G1 experiments but a much wider range ($R = 10^{-5.68}$–$10^{-7.63}$ mol m^{-2} s^{-1}) for the G2 experiments. Overall, the chemical composition of the initial and final solutions of both groups of experiments were maintained within 10%, indicating chemo-stat conditions were maintained during the course of each run.

The average $\delta^{26}Mg$ value of the master solutions was $-0.99 \pm 0.05‰$ (2SD, n = 9) for the G1, and $-0.92 \pm 0.08‰$ (2SD, n = 6) for the G2 experiments. The final solution $\delta^{26}Mg$ values averaged $-0.98 \pm 0.05‰$ (2SD, n = 9) for the G1, and $-0.92 \pm 0.06‰$ (2SD, n = 6) for the G2 experiments, indicating the Mg isotope composition of the master solutions remained constant over the course of each experiment. The offset in $\delta^{26}Mg$ value between the initial and final solution for each experiment never

Table 1
Solution chemistry for chemo-stat calcite precipitation experiments and chemical composition of calcite overgrowths.

Experiment No		Initial solution chemistry							Avg.	Seed	Precipitate	Mg	Final solution chemistry					Log R	$\Omega_{calcite}$	Exp.
		T (°C)	pCO_2 (%)	pH	[Ca] (mM)	[Mg] (mM)	Mg/Ca (mol/mol)	Alkalinity (meq)	*I* (mM)	mass (mg)	mass (mg)	content[a] (mol%)	pH	[Ca] (mM)	[Mg] (mM)	Mg/Ca (mol/mol)	Alkalinity (meq)	(mol/s/m^2)	Avg.	duration (h)
Group-1	RS7	25	5%	7.01	12.71	5.83	0.46	12.9	60.30	50.9	157.5	1.40	6.88	11.55	5.59	0.48	10.8	−6.19	4.50	53.32
	RS10	25	5%	7.02	12.01	5.20	0.43	12.9	56.59	50.1	161.6	1.42	6.99	10.60	5.21	0.49	10.3	−6.11	4.82	46.26
	RS17	25	5%	6.95	12.89	5.70	0.44	13.4	62.44	52.2	171.0	1.43	7.00	12.09	5.77	0.48	11.5	−6.11	5.01	47.08
	RS18	25	5%	6.95	12.81	5.50	0.43	13.6	59.70	51.4	196.5	1.44	6.75	11.32	5.52	0.49	11.4	−6.02	3.78	44.85
	RS23	25	5%	7.07	12.70	5.65	0.44	13.8	61.27	50.1	45.2	0.99	7.05	12.22	5.60	0.46	13.2	−5.65	6.80	4.52
	RS24	25	5%	6.90	12.84	5.56	0.43	13.9	61.45	500.6	165.1	0.96	6.96	12.06	5.54	0.46	12.9	−6.01	4.83	3.75
	RS25	25	5%	7.02	12.82	5.66	0.44	13.9	61.66	500.5	118.0	1.00	6.95	12.08	5.63	0.47	13.0	−5.98	5.62	2.48
	RS28	25	5%	6.75	12.71	5.63	0.44	13.6	60.73	5013.4	208.4	1.56	6.82	11.48	5.53	0.48	11.3	−6.45	2.92	1.30
	RS29	25	5%	6.86	12.78	5.69	0.45	14.2	58.92	5004.9	160.8	1.59	6.85	11.01	5.41	0.49	11.4	−6.33	3.66	0.77
Group-2	FU12	25	50%	6.37	13.25	9.90	0.75	24.0	80.46	57.7	125.7	2.79	6.35	11.58	9.83	0.85	20.5	−7.10	2.22	98.00
	FU48	25	3%	7.81	15.26	33.63	2.20	11.6	147.99	74.9	78.1	3.66	6.98	14.65	32.03	2.19	11.0	−7.26	5.28	68.25
	FU60	25	20%	6.61	15.09	33.37	2.21	22.3	153.44	60.0	28.8	6.50	6.60	14.89	32.28	2.17	21.6	−7.63	3.72	72.92
	FU98	25	60%	6.71	9.99	47.15	4.72	69.2	204.32	84.1	77.6	8.55	6.70	9.58	46.23	4.83	69.0	−7.10	6.64	41.24
	FU105	25	40%	6.96	9.94	42.87	4.31	71.1	185.93	67.4	263.8	10.41	6.90	8.22	41.33	5.03	68.3	−6.54	10.22	48.58
	FU125	25	100%	6.05	34.91	16.00	0.46	30.8	170.49	57.0	179.3	0.88	5.96	33.68	16.60	0.49	28.3	−5.68	2.92	5.34

[a] mol% of Mg in the overgrowth only.

Table 2
Magnesium isotopic compositions of calcite precipitation reactive solution and corresponding fractionation factors.

	Exp No	Initial solution				Final solution				Mg-calcite precipitate				Fractionation (cal-sol)			
		$\delta^{26}Mg$	2SD	$\delta^{25}Mg$	2SD	$\delta^{26}Mg$	2SD	$\delta^{25}Mg$	2SD	$\delta^{26}Mg$	2SD	$\delta^{25}Mg$	2SD	$\Delta^{26}Mg$	2SD	$\Delta^{25}Mg$	2SD
Group-1	RS7	−0.98	0.05	−0.51	0.03	−0.93	0.05	−0.47	0.03	−3.43	0.07	−1.77	0.04	−2.47	0.07	−1.28	0.05
	RS10	−0.96	0.05	−0.51	0.03	−1.00	0.05	−0.51	0.03	−3.38	0.07	−1.72	0.04	−2.40	0.07	−1.21	0.05
	RS17	−0.99	0.05	−0.53	0.03	−0.98	0.05	−0.52	0.03	−3.57	0.07	−1.82	0.05	−2.58	0.08	−1.30	0.05
	RS18	−0.98	0.05	−0.50	0.03	−0.99	0.05	−0.50	0.03	−3.55	0.07	−1.83	0.05	−2.57	0.08	−1.33	0.05
	RS23	−1.02	0.05	−0.53	0.03	−1.01	0.05	−0.52	0.03	−3.47	0.05	−1.84	0.05	−2.46	0.06	−1.32	0.06
	RS24	−0.99	0.05	−0.53	0.03	−1.03	0.04	−0.57	0.05	−3.49	0.05	−1.79	0.05	−2.48	0.06	−1.24	0.06
	RS25	−1.04	0.04	−0.55	0.05	−0.98	0.04	−0.51	0.05	−3.53	0.07	−1.79	0.05	−2.52	0.08	−1.25	0.06
	RS28	−1.01	0.05	−0.48	0.06	−0.98	0.07	−0.52	0.04	−3.45	0.07	−1.78	0.05	−2.46	0.08	−1.28	0.06
	RS29	−0.94	0.05	−0.47	0.04	−0.90	0.05	−0.43	0.04	−3.38	0.07	−1.74	0.05	−2.45	0.08	−1.29	0.06
Group-2	FU12	−0.93	0.07	−0.48	0.04	−0.91	0.07	−0.44	0.04	−3.60	0.07	−1.80	0.05	−2.68	0.09	−1.41	0.06
	FU48	−0.93	0.07	−0.46	0.04	−0.90	0.07	−0.48	0.04	−3.57	0.07	−1.75	0.05	−2.65	0.09	−1.35	0.06
	FU60	−0.91	0.07	−0.47	0.04	−0.92	0.07	−0.46	0.04	−3.60	0.07	−1.75	0.05	−2.69	0.09	−1.38	0.06
	FU98	−0.91	0.07	−0.45	0.04	−0.92	0.07	−0.45	0.04	−3.53	0.07	−1.80	0.05	−2.62	0.09	−1.39	0.06
	FU105	−0.91	0.07	−0.43	0.04	−0.88	0.07	−0.42	0.04	−3.26	0.07	−1.66	0.05	−2.36	0.09	−1.24	0.06
	FU125	−0.92	0.05	−0.48	0.04	−0.97	0.05	−0.49	0.04	−3.63	0.07	−1.85	0.05	−2.69	0.08	−1.36	0.06

exceeded 0.06‰, which is lower than the analytical precision. This is expected given that the amount of Mg incorporated in the overgrowths is generally less than 1.2% of the total aqueous Mg in the reactive solutions and most of the aqueous Mg is retained.

3.2. Chemical and isotopic composition of the calcite precipitates

XRD diffractograms of the final solids indicate that calcite and Mg-calcite are the only mineralogical phases present and no other phases such as aragonite or vaterite are detected. The weight of the overgrowth ranges from 28.8 to 263.8 mg, while the percentage of overgrowth relative to total recovered solids in each experiment ranges from 3.1 to 79.6 wt.% (see Table 1 for seed and precipitate weights). Crystal surfaces of the precipitates are smooth to rough with a various density of macrosteps and 2-D nucleation islands, whereas the seed material typically display smooth flat surfaces and euhedral crystal habit devoid of other surface feature, e.g., macrosteps and nucleation centers. The mole percentage of $MgCO_3$ in the overgrowth ranges from 0.96 to 1.59 mol% for the G1 experiments, and from 0.88 to 10.41 mol% for the G2 experiments.

The overgrowths in the G1 experiments exhibit limited variations in δ^{26}Mg value, ranging from −3.57 to −3.38‰ (±0.07, 2SD) (Table 2). Because the seed used in the G1 experiments contains no detectable Mg, the observed δ^{26}Mg value of the final solid is representative of the Mg-calcite overgrowth and no correction was required for the contribution of Mg from the seed material. However, as previously mentioned, five runs in the G2 experiments used Mg-bearing seed with one exception (FU125) that used the same Mg-free seed as those in the G1 experiments. Therefore, it is necessary to correct for the isotopic composition of Mg in the seed for five of the G2 runs. For these runs, the δ^{26}Mg value of the newly formed Mg-calcite precipitate is calculated using the following equation:

$$\delta^{26}Mg_{over} = \frac{\delta^{26}M_{bulk} \cdot X_{bulk} - \delta^{26}Mg_{seed} \cdot X_{seed}}{X_{over}} \quad (4)$$

where X_{seed}, X_{over}, and X_{bulk} are the mole fraction of Mg in the seed, overgrowth, and the bulk solid recovered at the end of the experiment, respectively. X_{seed} and X_{bulk} are determined by the Mg content in the seed and the bulk solid from ICP-AES analysis, which were used to calculate the X_{over}. The $\delta^{26}Mg_{seed}$ value is the Mg isotopic composition of the Mg-bearing seed and was measured to be −3.02 ± 0.04‰ (2SD, n = 6). $\delta^{26}Mg_{bulk}$ refers to the measured bulk solids of calcite precipitates with the seed material. The corrected values for the overgrowth only with error-propagated uncertainties are reported in Table 2. Most of the corrected δ^{26}Mg values for the Mg-calcite precipitates in the G2 runs cluster around −3.58 ± 0.07‰ (2SD, n = 4), except for FU105, which yields a δ^{26}Mg value of −3.26 ± 0.07‰. The run with Mg-free seed (FU125) yields a δ^{26}Mg value of −3.63 ± 0.07‰.

The Mg isotope fractionations between Mg-calcite and reactive solution ($\Delta^{26}Mg_{cal\text{-}sol}$) display limited variation for the G1 experiments (Table 2), ranging from −2.58 to −2.40‰, despite the wide range of calcite overgrowth mass relative to the seed mass (~3 to ~80%). For the G2 experiments with relatively large variations in aqueous chemical composition and reaction rate, the isotope fractionations between the newly formed calcite overgrowth and aqueous Mg (−2.69 to −2.36‰) are similar to the range of the G1 experiments.

3.3. Crystal morphology, texture, and form

The G1 experiments were conducted under identical chemical conditions but with various amounts of calcite seed consisting of {104} rhombohedra (Fig. 2A). The seed crystals have smooth flat faces with no evidence for macrosteps or secondary nucleation features. For the experiments run at a solid/solution ratio of 10^4 mg L^{-1} (RS28, 29) the mass of overgrowth was limited to 3–4 wt.%, and SEM images revealed that the overgrowths maintained a {104} rhombohedral form with smooth flat surfaces that displayed evidence of 2-D nucleation domains characterized by shallow macrosteps (Fig. 2B). Notable is a lack of growth features along the edges and corners of rhombohedra. At the intermediate solid/solution ratio of 10^3 mg L^{-1} (RS24, 25), the mass of overgrowth was 19–25 wt.% (Fig. 2C). The overgrowths still maintain a gross {104} rhombohedral form but steep-sided macrosteps dominated the surface of crystal faces and there was such little growth along the edges and corners of the rhombohedra that new crystal faces and forms begin to emerge. Finally, for the experimental runs at the lowest solid/solution ratio of 10^2 - mg L^{-1} (RS7, 10, 17, 18) and the highest percentage of overgrowth (76–79 wt.%), the overgrowths no longer displayed (104) rhombohedral faces and other rhombohedral forms {0*kl*} become prevalent (Fig. 2D).

All of our G2 experiments were conducted under a similar solid/solution ratio (~10^2 mg L^{-1}) but different solution Mg/Ca ratio with Mg-bearing (1.6 mol% Mg) rhombohedral calcite seed material (except FU125). For those experiments run at a Mg/Ca ratio ~0.5 (FU12, 125), the calcite surface overgrowths resemble those in the low solid/solution ratio G1 experiments (e.g., RS10 at 76 wt.% overgrowth Fig. 2D), regardless of whether the seed contained Mg (i.e., FU12) or not (i.e., FU125), with steep-sided and sharp-edged macrosteps (e.g., FU125 at 76 wt.% overgrowth; Fig. 2F). At the intermediate solution Mg/Ca ratio of ~2.2 (FU48, 60), a single (104) face remains on most crystals but all the other faces related by symmetry are lost (Fig. 2G), while at the highest Mg/Ca solution ratio of ~4.8 (FU98, 105), where the evolution of growth steps lead to the complete loss of the {104} form and aggregates of other {0*kl*} forms develop (Fig. 2H)

4. DISCUSSION

In this section, we first discuss various factors of solution chemistry and their impact on Mg incorporation into calcite and associated Mg isotope fractionation between aqueous Mg and solids, with particular focus on calcite growth mechanism and crystal morphology. We then use our results in conjunction with literature data to evaluate

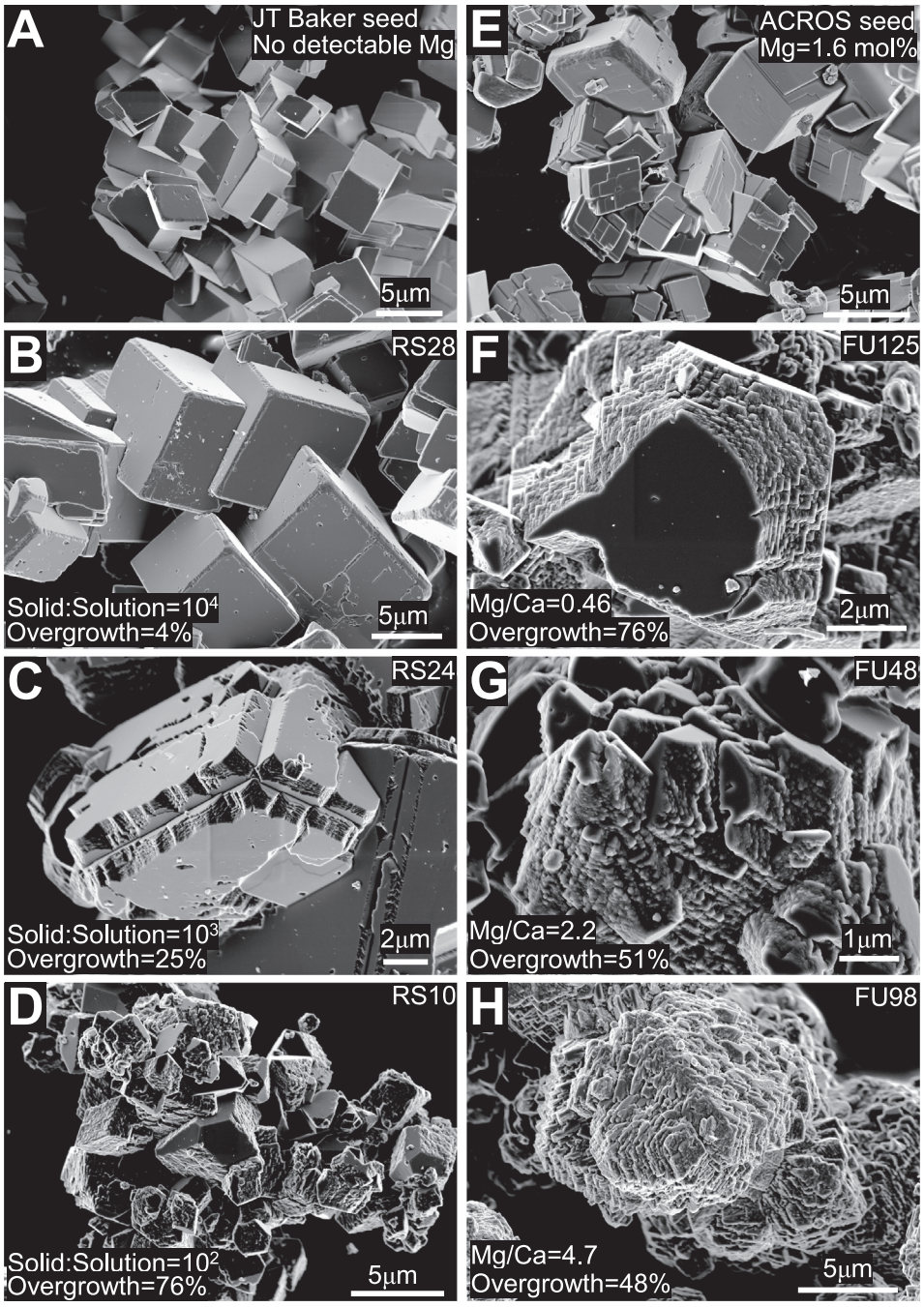

Fig. 2. Scanning electron photomicrographic images of calcite seed and overgrowth. (A) J.T.Baker™ seed used in G1 experiments and run FU125 of the G2 experiments. All crystals are Mg-free (<0.02 wt.%) (104) rhombohedra with smooth flat surfaces having a ~1–7 μm edge length and a specific surface area of 0.25 $m^2\ g^{-1}$. Calcite precipitates recovered from (B) exp. RS28 with solid/solution ratio of 10^4 mg L^{-1} and 4 wt.% overgrowth; (C) exp. RS24 with solid/solution ratio of 10^3 mg L^{-1} and 25 wt.% overgrowth; (D) exp. RS10 with solid/solution ratio of 10^2 mg L^{-1} and 76 wt.% overgrowth. The amount of overgrowth significantly affected the surface texture and crystal form, with clearly visible macro growth steps as the percentage of overgrowth increased; (E) ACROS seed material (1.6 mol% Mg) used in G2 experiments with a specific surface area of 0.78 $m^2\ g^{-1}$, except for FU125 which used Mg-free seed. Calcite precipitates recovered from (F) exp. FU125 with solution Mg/Ca molar ratio of 0.46 and 76 wt.% overgrowth, note the lack of growth on the (104) faces and the emergence of a new crystal form; (G) exp. FU48 with solution Mg/Ca molar ratio of 2.2 and 51 wt.% overgrowth, note the lack of (104) faces or forms; (H) exp. FU98 with solution Mg/Ca molar ratio of 4.7 and 48 wt.% overgrowth, note the complete lack of smooth faces and (104) faces or forms.

equilibrium Mg isotope fractionation at room temperature. Finally, we explore the potential implications of our results on carbonate Mg isotope applications.

4.1. Aqueous chemistry

4.1.1. Solution Mg/Ca ratio and Mg content in calcite precipitates

Early experimental studies suggest that the amount of Mg incorporated in calcite overgrowth is strongly correlated with the solution Mg/Ca ratio, rather than their absolute concentrations (Mackenzie et al., 1983; Mucci and Morse, 1983; Morse and Bender, 1990). Additionally, the presence of Mg in solution has been invoked to reduce the precipitation rate of calcite as the incorporation of trace elements induces lattice strain (Mucci et al., 1985; Zuddas and Mucci, 1994; Davis et al., 2000). Mucci and Morse (1983) suggested that the amount of Mg incorporated in calcite precipitated from seawater at 25 °C is controlled principally by the solution Mg/Ca ratio. This is likely ascribed to the fact that the calcite surface adsorbs more Mg ions at lower aqueous Mg/Ca ratios relative to higher ratios (Mucci and Morse, 1983).

Our G2 experiments conducted at different solution Mg/Ca molar ratios (0.5, 2.0, and 5.0) showed that Mg isotope fractionation during calcite precipitation is insensitive to solution Mg/Ca concentration ratio. A compilation of recent experimental studies on Mg isotope fractionation between aqueous solution and Mg-calcite precipitation also reveals a lack of meaningful correlation between $\Delta^{26}Mg_{cal\text{-}sol}$ values and aqueous Mg/Ca ratios (Fig. 3). Although experimental conditions vary between these studies, the $\Delta^{26}Mg_{cal\text{-}sol}$ usually displays a relatively wide range despite relatively limited variations in solution Mg/Ca ratio for individual experiments. This suggests some factor(s) other than solution Mg/Ca is responsible for the observed fractionation of Mg isotopes in calcite.

Similarly, the amount of Mg incorporated in calcite overgrowth (mol% Mg) as well as the amount of calcite overgrowth have negligible effects on Mg isotope fractionation in our experiments. This finding is consistent with most published work, as illustrated in Fig. 4. By contrast, the Mg isotopic fractionation data from Mavromatis et al. (2013) displayed positive correlations with both mol% Mg in overgrowth and relative degree (wt.%) of calcite overgrowth (Fig. 4). These observations suggest that other factors may have played a more important role in determining the Mg isotope fractionation during calcite precipitation in their experiments.

4.1.2. Ionic strength

The role of ionic strength (i.e., salinity) in determining di-valent metal isotope fractionation during calcite precipitation is still debated. For example, experiments in Mavromatis et al. (2013) display significant positive correlations between ionic strength and $\Delta^{26}Mg_{cal\text{-}sol}$ values ($R^2 = 0.91$). On the other hand, Tang et al. (2012) found that $\Delta^{44/40}Ca_{cal\text{-}sol}$ values were only weakly influenced by ionic strength and generally increased with higher ionic strength. The higher pH conditions (8.3) in the experiments of Tang et al. (2012) compared to pH ~ 6 in those of Mavromatis et al. (2013) could have resulted in more complexation, which may have affected the behavior of isotope fractionation. Additionally, the reported $\Delta^{26}Mg_{cal\text{-}sol}$ values in Li et al. (2012) were not correlated with ionic strength. Our experiments conducted at relatively low ionic strength (between 60 and 200 mM) yielded almost identical $\Delta^{26}Mg_{cal\text{-}sol}$ values, suggesting that Mg isotopic fractionation in our chemo-stat experiments was not impacted by changes in ionic strength.

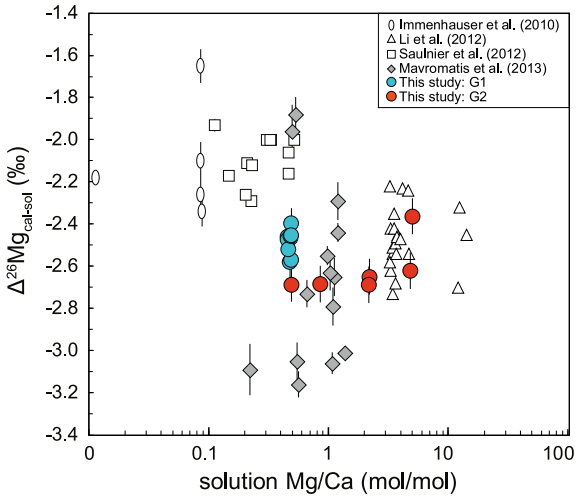

Fig. 3. Cross-plot of $\Delta^{26}Mg_{cal\text{-}sol}$ *versus* solution Mg/Ca molar ratio (log scale). G1 experiments were conducted at constant aqueous Mg/Ca molar ratio (~0.5) and the results are essentially indistinguishable. Three pairs of G2 experiments with aqueous Mg/Ca ratio of 0.5, 2.0, and 5.0 all display similar $\Delta^{26}Mg_{cal\text{-}sol}$ values. For Mg/Ca = ~5.0, the isotopic fractionation determined from FU105 is slightly smaller, but still within range of G1 experiments. The relatively high supersaturation for FU105 ($\Omega = 10.2$) may have facilitated the spontaneous nucleation of some carbonate of higher $\delta^{26}Mg$ value leading to the slightly reduced $\Delta^{26}Mg_{cal\text{-}sol}$ values for this experiment. Compilation of literature data also supports the hypothesis that solution Mg/Ca does not affect $\Delta^{26}Mg_{cal\text{-}sol}$ values (Immenhauser et al., 2010; Li et al., 2012; Saulnier et al., 2012; Mavromatis et al., 2013).

4.1.3. Speciation of aqueous Mg

Recent computational work by Schott et al. (2016) revealed that the aqueous speciation of Mg in reactive solutions can significantly affect the Mg isotopic composition of calcite, as the coordination number of Mg reduces from 6 in aqueous Mg^{2+} to 5 in Mg-bicarbonate and Mg-carbonate complexes. For example, at 25 °C, reduced partition function ratios indicate that the isotopic composition of Mg $(H_2O)_6^{2+}$ is 3.99‰ and 5.16‰ lower in $\delta^{26}Mg$ value than $MgHCO_3(H_2O)_4^+$ and $MgCO_3(H_2O)_4$, respectively (Schott et al., 2016). Hence $\delta^{26}Mg$ value of aqueous $Mg(H_2O)_6^{2+}$ would be lower than that of the bulk solution at isotope equilibrium. Assuming a constant $\delta^{26}Mg$ value for a series of solutions that have different fractions of $Mg(H_2O)_6^{2+}$, the magnitude of Mg isotope fractionation between calcite and the bulk solution would be greater for those with less $Mg(H_2O)_6^{2+}$ if only aqueous Mg is incorporated into calcite lattice. However, speciation calculations for the solutions

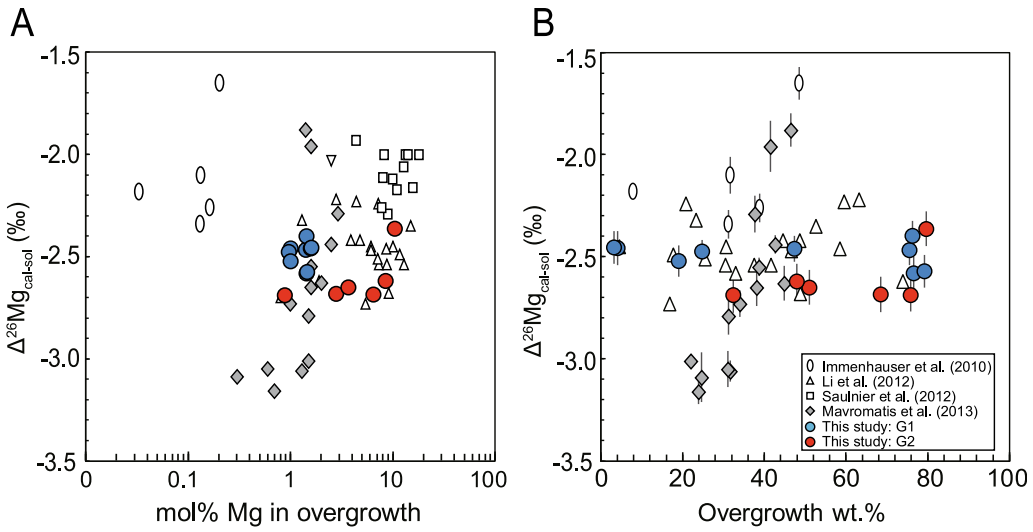

Fig. 4. Cross-plots of $\Delta^{26}Mg_{cal\text{-}sol}$ *versus* (A) mol% Mg in calcite overgrowth (log scale) and (B) amount of overgrowth as wt.%. The Mg content in calcite overgrowth ranges from 0.96 to 1.59 mol% for the G1 experiments and from 0.88 to 10.41 mol% for the G2 experiments. The amount of calcite precipitated during the course of the experiments ranges from 3.1 to 79.6 wt.%. Despite these relatively large variations, the $\Delta^{26}Mg_{cal\text{-}sol}$ values are relatively invariant, and no correlations were observed. Among the previously published data, only those data from Mavromatis et al. (2013) displayed positive correlations with either variable.

using the data reported in Mavromatis et al. (2013) suggest otherwise, and samples with a lower fraction of $Mg(H_2O)_6^{2+}$ (0.82 for CaMg113s and CaMg114s) yielded lower degrees of Mg isotope fractionation ($\Delta^{26}Mg_{cal\text{-}sol} = -1.88$ and -1.96‰, respectively) than samples with higher abundance of $Mg(H_2O)_6^{2+}$. This implies processes other than Mg speciation may play more important roles in the Mg-calcite-solution system.

The effect of aqueous Mg speciation is probably negligible in our experiments. This is because for most of our experiments, the fraction of $Mg(H_2O)_6^{2+}$ in reactive solution calculated using PHREEQC was ~0.91, and the $\Delta^{26}Mg_{cal\text{-}sol}$ values were within a narrow range. Two G2 experiments (FU98 and FU105) had lower fractions of $Mg(H_2O)_6^{2+}$ (~0.8) but only FU105 yielded a slightly higher $\Delta^{26}Mg_{cal\text{-}sol}$ value (−2.36‰) whereas the value for FU98 (−2.62‰) was indistinguishable from other G2 experiments (~−2.68‰). This slightly higher $\Delta^{26}Mg_{cal\text{-}sol}$ value for FU105 may be attributed to its much higher saturation state ($\Omega = 10.2$, Table 1) where the potential for spontaneous nucleation is greater.

4.2. Kinetic effect

Kinetic isotope fractionation during calcite precipitation (i.e., precipitation rate dependent isotope fractionation) has been observed for a number of divalent metal elements, including the alkaline earth element Ca, Sr, and Ba, and the transition metals Zn and Cd (Tang et al., 2008, 2012; Horner et al., 2011; DePaolo, 2011; Böhm et al., 2012; Nielsen et al., 2012; Schott et al., 2014; AlKhatib and Eisenhauer, 2017). As for Mg isotopes, the observations are more diverse with some studies showing strong kinetic isotope fractionation patterns (Immenhauser et al., 2010; Mavromatis et al., 2013) while other studies suggest no dependence on precipitation rate (Kisakürek et al., 2009; Li et al., 2012; Saulnier et al., 2012).

Our chemo-stat experiments conducted at 25 °C display no correlation between $\Delta^{26}Mg_{cal\text{-}sol}$ values and precipitation rate for either the G1 or G2 experiments (Fig. 5). For the G1 experiments, $\Delta^{26}Mg_{cal\text{-}sol}$ values were nearly identical, and the calculated calcite precipitation rate spans a relatively narrow range ($R = 10^{-5.65}$–$10^{-6.45}$ mol m^{-2} s^{-1}). For the G2 experiments, the precipitation rate displays a much wider range ($R = 10^{-5.68}$–$10^{-7.63}$ mol m^{-2} s^{-1}) yet the $\Delta^{26}Mg_{cal\text{-}sol}$ values are still identical (~−2.67 ± 0.06‰, 2SD, n = 5) with only one experiment (FU105) yielding a slightly higher $\Delta^{26}Mg_{cal\text{-}sol}$ value (−2.36 ± 0.06‰, 2SD), which may be attributed to its much higher saturation state.

By contrast, Immenhauser et al. (2010) and Mavromatis et al. (2013) reported rate-dependent Mg isotope fractionation during calcite precipitation with higher $\Delta^{26}Mg_{cal\text{-}sol}$ values at faster precipitation rate. However, this trend is opposite in sense to rate-dependent fractionations reported between calcite and solution for Ca and O isotopes (Tang et al., 2008; Watkins et al., 2013) where $\Delta^{44/40}Ca_{cal\text{-}sol}$ and $\Delta^{18}O_{cal\text{-}sol}$ decrease with increasing precipitation rate. Furthermore, the two sets of experiment by Immenhauser et al. (2010) and Mavromatis et al. (2013) were conducted at different temperatures, and temperature has been suggested to strongly affect Mg, Ca, and Sr isotopic fractionation (Tang et al., 2008; AlKhatib and Eisenhauer, 2017) with less Sr and Ca isotope fractionation at higher temperatures at similar precipitation rate. A similar relationship between temperature and fractionation values was also reported for Mg isotopes during calcite (Li et al., 2012), aragonite (Wang et al., 2013), and magnesite (Pearce et al., 2012) precipitation. However, calcite samples precipitated in Mavromatis et al. (2013) at 25 °C generally displayed a larger degree of Mg isotopic fractionation than

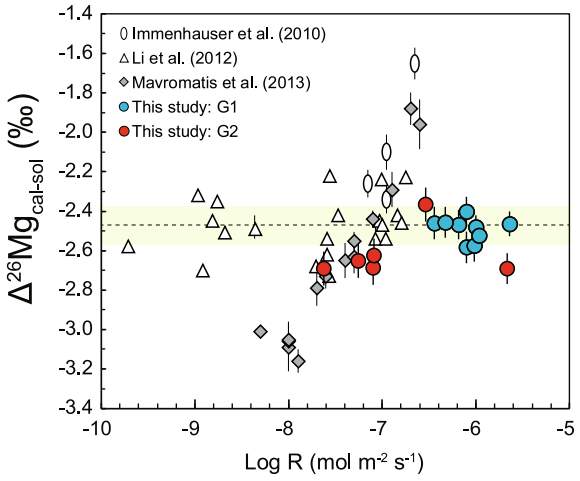

Fig. 5. Cross-plot of $\Delta^{26}Mg_{cal\text{-}sol}$ *versus* calcite precipitation rate (Log R). No correlation was observed in our G1 and G2 experiments. Similarly, Mg isotopic fractionation from Li et al. (2012) was not affected by precipitation rate. In contrast, Mavromatis et al. (2013) observed a strong correlation between $\Delta^{26}Mg_{cal\text{-}sol}$ values and precipitation rate. Calcite samples precipitated at 25 °C in Mavromatis et al. (2013) generally display higher $\Delta^{26}Mg_{cal\text{-}sol}$ values than those reported at 10.3 °C in Immenhauser et al. (2010) at similar precipitation rates, which is opposite in sense to the prediction of temperature-dependent isotopic fractionation. The estimated equilibrium $\Delta^{26}Mg_{cal\text{-}sol}$ value of -2.47 ± 0.09‰ (weighted average ± weighted 2SD, $n = 70$) from our study and literature data at 25 °C is represented by the dash line and yellow error envelope.

those formed at 10.3 °C by Immenhauser et al. (2010) over a similar range in precipitation rate, which is opposite in sense to the temperature dependence of a kinetically controlled reaction. Although the reported $\Delta^{26}Mg_{cal\text{-}sol}$ values and precipitation rates from Immenhauser et al. (2010) and Mavromatis et al. (2013) plot on a similar trend (Fig. 5), it is difficult to attribute this trend solely to precipitation rate, and other factors such as differences in experimental setup and calcite growth mechanisms must be considered.

4.3. Influence of crystal morphology on $\Delta^{26}Mg_{cal\text{-}sol}$

Reddy and Gaillard (1981) demonstrated that calcite precipitation can be influenced by solid/solution ratio so this variable may also affect Mg isotope fractionation relations. They concluded that rate constant for calcite was independent of solid/solution ratio above ~1000 mg L^{-1}, while below that value rate constant increased as solid/solution ratio decreased. This was explained as a result of additional surface area that arises through competition between growth on the calcite seed crystal surface and secondary surface nucleation sites. At relatively low solid/solution ratios, final solids show well-developed macro growth steps on the crystal faces, and the number and height of the macrosteps increase as solid/solution ratio decreases. At high solid/solution ratios, the large available growth surface area relative to the amount of material to be deposited from solution leads to relatively few growth steps while at low solid/solution ratios dense arrays of macrosteps form as well as evidence for surface and edge nucleation. The overgrowths in our experiments show similar characteristics and can be interpreted within the context of solid/solution ratio.

Our G1 experiments were conducted with various amounts of calcite seed material under identical chemical conditions to explore the influence of solid/solution ratio on calcite crystal morphologies and Mg isotopic fractionation. SEM images reveal that the morphologies of calcite overgrowths vary from a {104} rhombohedral form with 2-D nucleation domains and shallow macrosteps in high solid/solution ratio experiments to a gross {104} rhombohedral form with steep-sided macrosteps dominating the surface of crystal faces at the intermediate solid/solution ratio, to rhombohedral forms {0*kl*} without (104) rhombohedral faces at the lowest solid/solution ratio. Nevertheless, the measured $\Delta^{26}Mg_{cal\text{-}sol}$ values for the 9 runs in the G1 experiments display a limited range of values from −2.58 to −2.40‰ with an average of -2.49 ± 0.12‰ (2SD, $n = 9$). This suggest that differences in calcite crystal morphology induced by variable solid/solution ratios have little impact on the Mg isotope fractionation between solid and solution.

Additionally, solution Mg/Ca has also been shown to affect calcite crystal morphologies because the incorporation of Mg into calcite crystals causes strain accumulation at the growth step boundaries and can significantly modify the crystallographically controlled growth step directions (Folk, 1974; Davis et al., 2004). Davis et al (2004) suggested that at high Mg/Ca solution ratios, the edges of growth steps roughen, and growth spirals become more anisotropic. The G2 experiments were carried out under a similar solid/solution ratio (~10^2 mg L^{-1}) to the G1 experiments but different solution Mg/Ca ratio (ranging from ~0.5 to ~5.0) with Mg-bearing (1.6 mol% Mg) rhombohedral calcite seed material (except for FU125). Our results are consistent with Davis et al (2004) and SEM images illustrate the difference between calcite surface overgrowths at low Mg/Ca ratio relative to those at high Mg/Ca ratio conditions (Fig. 2). The crystal surfaces at low Mg/Ca ratio display steep-sided and sharp-edged macrosteps, whereas those precipitated at the highest Mg/Ca solution ratio of ~5.0 completely lose the {104} form and aggregates of other {0*kl*} forms develop. Despite the large contrast in calcite crystal morphological features, the observed $\Delta^{26}Mg_{cal\text{-}sol}$ values are similar (−2.69 to −2.36‰) and in the same range of those from the G1 experiments.

The SEM results from our chemo-stat experiments are consistent with the findings of Reddy and Gaillard (1981) and Davis et al. (2004) and suggest that solid/solution ratio and Mg/Ca ratio influence the physical character of the precipitates. As the available surface area for heterogeneous growth decreases, the driving force of precipitation at a constant solution chemistry requires a unit mass of carbonate to deposit over a smaller surface area. This results in a competition between surface growth (e.g., spiral growth along screw dislocations) and 2-D nucleation. All of the precipitates from the G1 and G2 experiments display evidence for 2-D nucleation, although the extent and nature

may have varied depending on solid/solution ratio. Nevertheless, despite these fundamental changes in crystal form and texture, $\Delta^{26}Mg_{cal\text{-}sol}$ values for these experiments are indistinguishable within our analytical uncertainty, suggesting that a 2-D nucleation growth mechanism is insensitive to growth rate and does not influence Mg-isotope fractionation. In comparison, the SEM image of calcite overgrowth in Mavromatis et al. (2013; their Fig. 4B) display the same {104} rhombohedral form as the seed material, with no evidence of macroscopic growth steps or 2-D nucleation islands on any crystal face, suggesting that their precipitates may have formed by a spiral growth mechanism that experienced kinetic isotopic effect. This is further supported by the experimental approach adopted by Mavromatis et al. (2013). Table A2 in the Supplemental material summarizes the main differences in experiment condition between our study, and those of Li et al. (2012) and Mavromatis et al. (2013). In the experiments of Mavromatis et al. (2013), seed crystals were introduced to a solution in chemical equilibrium with pure calcite. Titrants were added to increase the concentration of dissolved constituents and promote the growth of a solid phase at very low levels of supersaturation where spiral growth mechanisms are predominant. This near chemical equilibrium growth process is well characterized in flow-through cell studies of calcite growth that utilize atomic force microscopy (AFM) to characterize the evolution of growing crystal surfaces at almost atomic resolution (Davis et al., 2000, 2004; Teng et al., 1999, 2000; Wasylenki et al., 2005).

4.4. Influence of growth mechanism

Growth of calcite crystals from supersaturated solutions is initiated by nucleation that forms new crystallization centers. The formation of nuclei in the absence of any foreign particles or surfaces is considered a homogeneous nucleation, while a heterogeneous nucleation process involves the presence of a pre-existing surface (Garside, 1982). It is widely accepted that homogeneous (spontaneous) and seeded growth (heterogeneous) nucleation involve different reaction mechanisms (Garside, 1982; De Yoreo and Vekilov, 2003). It is perhaps not surprising that experimentally determined $\Delta^{26}Mg_{cal\text{-}sol}$ values reported by Immenhauser et al. (2010) and Saulnier et al. (2012) were, on average, higher (mean = −2.10‰) as their experiments were conducted in the absence of calcite seed. The initial spontaneous nucleation of a solid phase may not discriminate among Mg-isotopologues during the precipitation process. However, higher values of $\Delta^{26}Mg_{cal\text{-}sol}$ reported in Mavromatis et al. (2013) may not be explained by this mechanism as they precipitated Mg-calcite overgrowths on calcite seed material through a heterogeneous growth process.

Moreover, crystal step propagation can be influenced by solution saturation state (Teng et al., 2000). At lower degrees of supersaturation ($\Omega < 2.2$), calcite precipitation is dominated by spiral growth initiated by surface imperfections from screw dislocations. When $\Omega > 2.2$, direct nucleation on the surfaces as 2-D islands becomes increasingly important (Teng et al., 1999, 2000). The transition from spiral growth to 2-D-nucleation may have a strong impact on the fractionation of Ca isotopes (Nielsen et al., 2012). All experiments in Mavromatis et al. (2013) were performed at relatively low supersaturation ($\Omega < 3.3$), and most of which were below 2.5, whereas most of our G1 and G2 experiments and those from Li et al. (2012) were conducted at higher levels of supersaturation. Nielsen et al. (2012) suggested that the fractionation of Ca isotopes during spiral growth is more prominent than for 2-D nucleation. Assuming Mg isotope fractionation is also affected by different growth mechanism, it is thus plausible that kinetic effect of Mg isotope fractionation was dominated by spiral growth in Mavromatis et al. (2013), which was mainly controlled by surface adsorption and dehydration processes and preferential incorporation of Mg in acute-stepped flanks of growth hillocks. By contrast, the chemo-stat experiment of our study, and the free-drift experiments in Li et al. (2012) may have been dominated by 2-D-nucleation, where a structural unit such as a dimer ($MgCO_3$ or $MgHCO_3^-$) may participate in the precipitation reaction. As such 2-D nucleation may be insensitive to precipitation rate effects on Mg isotope fractionation.

In addition, the presence of Mg in the calcite seed prior to precipitation does not seem to affect the Mg isotopic fractionation between solid and aqueous Mg. This is supported by the evidence that the overgrowth of FU12 (Mg-bearing seed) and FU125 (Mg-free seed) from the G2 experiments exhibit identical $\Delta^{26}Mg_{cal\text{-}sol}$ values (−2.68 ± 0.09‰ for FU12 and −2.68 ± 0.08‰ for FU125), suggesting that the Mg isotope fractionation during calcite precipitation is independent of pre-existing Mg in the calcite lattice.

4.5. Equilibrium fractionation from experimental and theoretical studies

The $\Delta^{26}Mg_{cal\text{-}sol}$ values in our experiments conducted at 25 °C were not affected by solution chemistry, precipitation kinetics or crystal shape/form so they likely reflect equilibrium Mg isotopic fractionation, yielding $\Delta^{26}Mg_{cal\text{-}sol}$ values that range from −2.69 to −2.36‰ with an average of −2.54 ± 0.22‰ (2SD, $n = 15$). This is consistent with the average values for five experiments at 22 °C in Li et al. (2012: −2.56 ± 0.19‰, 2SD, n = 5), and the value of −2.4 ± 0.2‰ (2SD, n = 5) at 25 °C reported by Kisakürek et al. (2009).

Equilibrium isotope fractionation is temperature-dependent because of vibration energies in crystals. The fractionation of Mg isotopes as a function of temperature was observed from natural carbonate samples and experimental studies. Galy et al. (2002) first studied $\delta^{26}Mg$ values for speleothem carbonate and associated drip water in four caves under various climate conditions. The $\Delta^{26}Mg_{cal\text{-}sol}$ fractionations varied from −2.57 to −2.80‰, and this was interpreted to reflect near equilibrium conditions as it was weakly correlated with annual mean temperature in the range of 4° to 18 °C. Extrapolating the temperature dependence relationship reported in Galy et al. (2002) to 25 °C results in $\Delta^{26}Mg_{cal\text{-}sol}$ fractionation factors between −2.50 and −2.61‰, similar to the mean value in our study.

The previously determined values from natural speleothem samples and laboratory experiments are in close agreement with our experimental results and likely represent equilibrium Mg isotopic fractionation (Fig. 6).

Immenhauser et al. (2010) determined Mg isotopic fractionation factors from speleothems and waters in Bunker Cave (mean temperature ~10.3 °C). Their samples fell into two groups:1) Group 1 samples represent bulk speleothems and their average $\Delta^{26}Mg_{cal\text{-}sol}$ was determined to be −2.61‰, whereas 2) Group 2 samples were taken from the surface of speleothems and they yielded higher values with an average of −1.88‰. The Group 2 samples were interpreted to have precipitated at a faster precipitation rate and did not attain Mg isotopic equilibrium (Immenhauser et al., 2010). It is worth noting that the average $\Delta^{26}Mg_{cal\text{-}sol}$ value for their Group 1 samples is well within the range of our estimated equilibrium fractionation even after correcting for the temperature effect ($\Delta^{26}Mg_{cal\text{-}sol} = -0.158 \times 10^6/T^2 - 0.74$, Li et al., 2012). By contrast, experiments by Immenhauser et al. (2010) and Saulnier et al. (2012) found slightly higher values for $\Delta^{26}Mg_{cal\text{-}sol}$, (mean = −2.10‰) which may have resulted from the spontaneous nucleation process they employed to generate precipitate. Despite large variations in $\Delta^{26}Mg_{cal\text{-}sol}$ values determined by Mavromatis et al. (2013), the mean value (−2.66‰) is still within our estimated range of equilibrium fractionation factors between calcite and solution. Additionally, in a recent study of amorphous calcium carbonate (ACC) transformation by Mavromatis et al. (2017b), in one of their experiments conducted at relatively low supersaturation where no ACC was formed and only Mg-calcite precipitated, the measured $\Delta^{26}Mg_{cal\text{-}sol}$ value was −2.36‰, which is also within our estimated range of equilibrium fractionation. Another study by Mavromatis et al. (2017a) investigated the effects of organic ligands on Mg partitioning and Mg isotope fractionation during calcite precipitation at 25 °C. They concluded that the presence of organic ligands, with the exception of citric acid, does not significantly affect the Mg isotopic fractionation and the observed fractionation factor ranged from −2.42 to −2.62 with a mean value of −2.51 ± 0.11‰ (2SD, $n = 15$).

Combining all the aforementioned studies on laboratory experiments without prominent kinetic effect, and natural cave samples after correcting for temperature effect using the relationship reported in Li et al. (2012) with our current study, we suggest that equilibrium Mg isotopic fractionation between Mg-calcite and its precipitating solution at 25 °C is likely −2.47 ± 0.09‰ (weighted average ± weighted 2SD, $n = 70$, Galy et al., 2002; Kisakürek et al., 2009; Immenhauser et al., 2010; Li et al., 2012; Mavromatis et al., 2017a, 2017b). The experimental results of Immenhauser et al. (2010) and the study by Saulnier et al. (2012) were not included because they were conducted without seed material and the initial spontaneous nucleation may have resulted in slightly different Mg isotope fractionation pathways.

The estimated equilibrium fractionation factor, however, is significantly higher than those determined between calcite solids and free Mg ion from theoretical calculations using *ab initio* methods (Rustad et al., 2010; Schauble, 2011; Pinilla et al., 2015; Schott et al., 2016; Wang et al., 2017, 2019; Gao et al., 2018) (Fig. 7). Although these first-principle studies generally agree on the direction of fractionation for carbonate minerals, the magnitudes of which vary significantly from one study to another. For example, at 25 °C, the $\Delta^{26}Mg_{cal\text{-}sol}$ calculated for infinite dilute Mg in calcite from density function theory (DFT) using BP86 and B3LYP models are −3.63 and −5.33‰, respectively

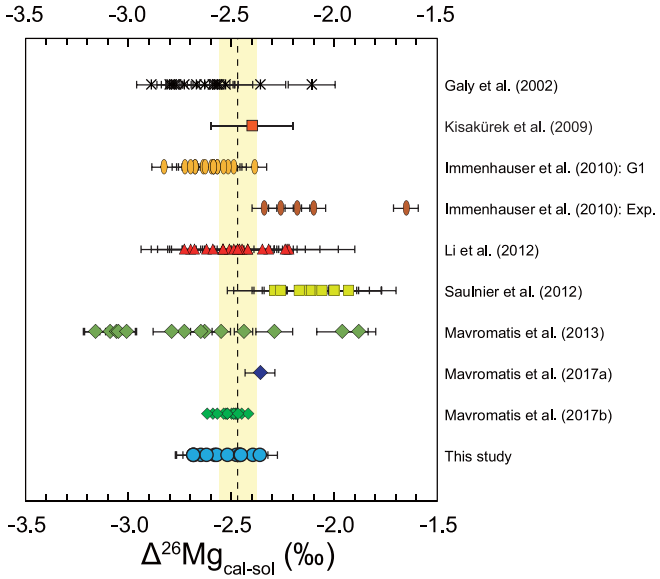

Fig. 6. The distribution of $\Delta^{26}Mg_{cal\text{-}sol}$ values from our study and those reported in the literature that include natural speleothems and experimental work (Galy et al., 2002; Kisakürek et al., 2009; Immenhauser et al., 2010; Li et al., 2012; Saulnier et al., 2012; Mavromatis et al., 2013, 2017). The overall range of $\Delta^{26}Mg_{cal\text{-}sol}$ values is from −3.16 to −1.65‰. Excluding those affected by kinetic isotope effect, the integrated equilibrium $\Delta^{26}Mg_{cal\text{-}sol}$ value at 25 °C is −2.47 ± 0.09‰ (weighted average ± weighted 2SD, $n = 70$), as indicated by the dashed line and yellow error envelope.

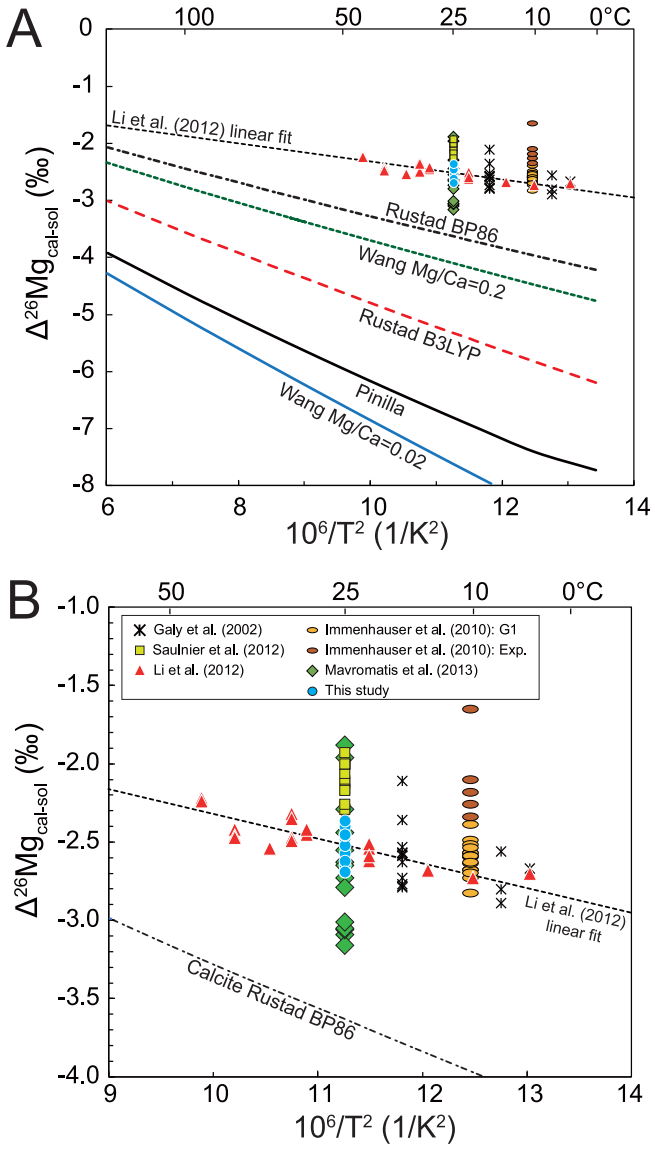

Fig. 7. (A) Comparison of theoretical calculated Mg isotopic fractionation factors for calcite with those obtained from natural carbonate samples and laboratory experiments. The fractionation factor by Rustad et al. (2010) was calculated using two different models (BP86 and B3LYP). Wang et al. (2019) calculated two calcite fractionation factors with different Mg/Ca molar ratio (0.2 and 0.02). Solid black line represents $\Delta^{26}Mg_{cal\text{-}sol}$ values calculated by Pinilla et al. (2015). Data from natural observations and experiments were significantly higher than predicted values and generally clustered around the linear fit temperature-dependent curve from Li et al. (2012). (B) A close-up view of the $\Delta^{26}Mg_{cal\text{-}sol}$ values determined from natural samples and experimental work. Dotted line is the linear fit curve from Li et al. (2012).

(Rustad et al., 2010). Pinilla et al. (2015) performed path integral molecular dynamics simulations and their calculated $\Delta^{26}Mg_{cal\text{-}sol}$ at 25 °C is −6.81‰ for calcite with 6.25 mol% Mg.

The potential exists that theoretical equilibrium isotopic fractionation factors are dependent on the Mg content of calcite, as atomic relaxation leads to slightly different Mg-O bond lengths (Pinilla et al., 2015; Wang et al., 2019). For example, calculated $\Delta^{26}Mg_{cal\text{-}sol}$ values increase by 1.2‰ at 25 °C when the Mg content in calcite decreases from 6.25 to 3.13 mol% (Pinilla et al., 2015). Similarly, the calculated $\Delta^{26}Mg_{cal\text{-}sol}$ by Wang et al. (2019) increases from −7.64‰ with 2 mol% Mg to −4.12‰ with 20 mol% Mg at 25 °C. However, concentration effects are not observed in our experiments or previously published experimental work (Fig. 7) and further studies are needed to resolve the discrepancies between theoretical and empirical studies.

4.6. Implication for carbonate Mg isotopes application

Our experiments, together with previously published work, suggest that $\Delta^{26}Mg_{cal\text{-}sol}$ is −2.47 ± 0.09‰ (weighted average ± weighted 2SD, $n = 70$) at 25 °C, independent of solution Mg/Ca ratio, precipitation rate, Mg content in calcite, or changes in crystal form and texture. Therefore, the

Mg isotopic composition of Mg-bearing calcite provides insights into the environment and fluids of its formation and may serve as a cornerstone to understand many geological processes (e.g., paleoenvironment and paleoclimate change, evolution of seawater Mg/Ca ratio, continental weathering, diagenesis, CO_2 sequestration, deep carbon cycle). Notwithstanding, kinetic effect may still influence the Mg isotope composition of calcite grown solely by a spiral growth mechanism, but further work is required to document this potential effect.

Studies on marine biogenic carbonate have documented large variations of δ^{26}Mg values (>4.5‰) across a variety of carbonate-secreting organisms, such as foraminifera, corals, echinoids, brachiopods, bivalves, and coccoliths (Chang et al., 2004; Pogge von Strandmann et al., 2014; Hippler et al., 2009; Ra et al., 2010; Wombacher et al., 2011; Saenger and Wang, 2014). Biomineralization processes can be species-specific since parameters such as pH, salinity, bonding with biomolecules, preferred mineralogy, and enzymatic activities likely vary between different organismal groups. These vital effects potentially influence the Mg isotopic composition of biogenic carbonates. Understanding the equilibrium isotopic fractionation of inorganic calcite formation is thus the first step towards unraveling more complicated and convoluted biomineralization processes.

In addition, the formation of calcium carbonate is closely associated with the global carbon cycle. Chemical weathering of carbonate rocks can have significant impact on long-term seawater Mg isotope composition and the evolution of oceanic Mg/Ca over geologic time (Berg et al., 2019). Some portion of marine carbonates are brought to depth via subduction, and the fluids released during partial melting and metasomatism could lead to distinct Mg isotopic signatures. A better constrained $\Delta^{26}Mg_{cal\text{-}sol}$ value will help to make better estimates of deep carbon fluxes.

5. CONCLUSIONS

The Mg isotope fractionation between synthetic calcite and solution was determined at room temperature over a range of parameters using the chemo-stat approach. The results suggest that $\Delta^{26}Mg_{cal\text{-}sol}$ value is insensitive to changes in solution pH, Mg/Ca ratio, solid/solution ratio, overgrowth percent, pCO_2, Mg content in calcite, and precipitation rate. Nine experiments conducted at identical chemical conditions but differing solid/solution ratio and duration produced various amount of calcite overgrowth by a 2-D growth mechanism, with the overgrowths displaying different surface textures and crystal morphologies. The $\Delta^{26}Mg_{cal\text{-}sol}$ values for these runs are indistinguishable within analytical uncertainty suggesting that changes in crystal texture and form do not influence Mg isotope fractionation relations in this system. The kinetic effect observed in one previous study (Mavromatis et al., 2013) may be due to a fundamental difference in growth mechanism (i.e., spiral growth) but additional work is required to document this effect.

Overall, the experiments of this study yielded an average $\Delta^{26}Mg_{cal\text{-}sol}$ of -2.54 ± 0.22‰ (error weighted average $\pm$ 2SD, $n = 15$) at 25 °C, which is consistent with previously determined values from natural speleothem system and the majority of all previous other laboratory experiments. Combining our estimate with the literature data yield a weighted average value of -2.47 ± 0.09‰ (weighted average $\pm$ weighted 2SD, $n = 70$) for equilibrium Mg isotopic fractionation between Mg-calcite and its forming solution at room temperature. Our results help pave ways for using carbonate Mg isotopes as a tool to investigate a variety of processes including paleoclimate reconstruction, deep carbon cycling, and vital effects during biomineralization of marine organisms.

Declaration of Competing Interest

The authors declare that they have no known competing financial interests or personal relationships that could have appeared to influence the work reported in this paper.

ACKNOWLEDGEMENT

We thank Sylvia Riechelmann and one anonymous reviewer for their insightful and critical comments, which significantly improved the manuscript. The careful and efficient editorial handing by AE Adrian Immenhauser is greatly appreciated. We would also like to thank Bing-Yu Lee for assistance on sample processing and column chemistry for Mg isotope analyses, Heng-Ci Tian, Yan Hu, and Mingzhu Liu for discussion and constructive comments, Jon Tonner for assistance on PHREEQC, and the Quantachrome's Material Characterization Laboratory for providing surface area analyses of calcite seed material. This work was financially supported by National Science Foundation EAR-1747706, NASA Astrobiology Institute grant NNA13AA94A, the Summer Research Fellowship program through the Office of Undergraduate Research at Furman University, the Spanish Government FEDER projects CGL2016-75679-P and CGL2016-79458-P, and the Dutch Research Council (NWO) Origins Center project 190438131.

APPENDIX A. SUPPLEMENTARY MATERIAL

Supplementary data to this article can be found online at https://doi.org/10.1016/j.gca.2020.04.033.

REFERENCES

AlKhatib M. and Eisenhauer A. (2017) Calcium and strontium isotope fractionation in aqueous solutions as a function of temperature and reaction rate; I. Calcite. *Geochim. Cosmochim. Acta* **209**, 296–319.

Berg R. D., Solomon E. A. and Teng F.-Z. (2019) The role of marine sediment diagenesis in the modern oceanic magnesium cycle. *Nat. Commun.* **10**, 4371.

Böhm F., Eisenhauer A., Tang J., Dietzel M., Krabbenhöft A., Kisakürek B. and Horn C. (2012) Strontium isotope fractionation of planktic foraminifera and inorganic calcite. *Geochim. Cosmochim. Acta* **93**, 300–314.

Buhl D., Immenhauser A., Smeulders G., Kabiri L. and Richter D. K. (2007) Time series δ^{26}Mg analysis in speleothem calcite: Kinetic versus equilibrium fractionation, comparison with other proxies and implications for palaeoclimate research. *Chem. Geol.* **244**, 715–729.

Chang V. T. C., Williams R. J. P., Makishima A., Belshawl N. S. and O'Nions R. K. (2004) Mg and Ca isotope fractionation during $CaCO_3$ biomineralisation. *Biochem. Biophys. Res. Commun.* **323**, 79–85.

Davis K. J., Dove P. M. and De Yoreo J. J. (2000) The role of Mg^{2+} as an impurity in calcite growth. *Science* **290**, 1134–1137.

Davis K. J., Dove P. M., Wasylenki L. E. and De Yoreo J. J. (2004) Morphological consequences of differential Mg^{2+} incorporation at structurally distinct steps on calcite. *Am. Mineral.* **89**, 714–720.

De Yoreo J. J. and Vekilov P. G. (2003) Principles of crystal nucleation and growth. *Rev. Mineral. Geochem.* **54**, 57–93.

DePaolo D. J. (2011) Surface kinetic model for isotopic and trace element fractionation during precipitation of calcite from aqueous solutions. *Geochim. Cosmochim. Acta* **75**, 1039–1056.

Elderfield H. and Ganssen G. (2000) Past temperature and $\delta^{18}O$ of surface ocean waters inferred from foraminiferal Mg/Ca ratios. *Nature* **405**, 442–445.

Folk R. L. (1974) The natural history of crystalline calcium carbonate; effect of magnesium content and salinity. *J. Sediment. Res.* **44**, 40–53.

Galy A., Bar-Matthews M., Halicz L. and O'Nions R. K. (2002) Mg isotopic composition of carbonate: insight from speleothem formation. *Earth Planet. Sci. Lett.* **201**, 105–115.

Gao C., Cao X., Liu Q., Yang Y., Zhang S., He Y., Tang M. and Liu Y. (2018) Theoretical calculation of equilibrium Mg isotope fractionations between minerals and aqueous solutions. *Chem. Geol.* **488**, 62–75.

Garside J. (1982) Nucleation. In *Biological Mineralization and Demineralization* (ed. G. H. Nancollas). Springer, Berlin Heidelberg, Berlin, Heidelberg, pp. 23–35.

Higgins J. A. and Schrag D. P. (2010) Constraining magnesium cycling in marine sediments using magnesium isotopes. *Geochim. Cosmochim. Acta* **74**, 5039–5053.

Higgins J. A. and Schrag D. P. (2012) Records of Neogene seawater chemistry and diagenesis in deep-sea carbonate sediments and pore fluids. *Earth Planet. Sci. Lett.* **357–358**, 386–396.

Higgins J. A. and Schrag D. P. (2015) The Mg isotopic composition of Cenozoic seawater–evidence for a link between Mg-clays, seawater Mg/Ca, and climate. *Earth Planet. Sci. Lett.* **416**, 73–81.

Hippler D., Buhl D., Witbaard R., Richter D. K. and Immenhauser A. (2009) Towards a better understanding of magnesium-isotope ratios from marine skeletal carbonates. *Geochim. Cosmochim. Acta* **73**, 6134–6146.

Horner T. J., Rickaby R. E. M. and Henderson G. M. (2011) Isotopic fractionation of cadmium into calcite. *Earth Planet. Sci. Lett.* **312**, 243–253.

Hu Y., Harrington M. D., Sun Y., Yang Z., Konter J. and Teng F. Z. (2016) Magnesium isotopic homogeneity of San Carlos olivine: a potential standard for Mg isotopic analysis by multi-collector inductively coupled plasma mass spectrometry. *Rapid Commun. Mass Spectrom.* **30**, 2123–2132.

Immenhauser A., Buhl D., Richter D., Niedermayr A., Riechelmann D., Dietzel M. and Schulte U. (2010) Magnesium-isotope fractionation during low-Mg calcite precipitation in a limestone cave – field study and experiments. *Geochim. Cosmochim. Acta* **74**, 4346–4364.

Kisakürek B., Niedermayr A., Müller M., Taubner I., Eisenhauer A., Dietzel M., Buhl D., Fietzke J. and Erez J. (2009) Magnesium isotope fractionation in inorganic and biogenic calcite. *Geochim. Cosmochim. Acta* **73**, A663.

Li W., Chakraborty S., Beard B. L., Romanek C. S. and Johnson C. M. (2012) Magnesium isotope fractionation during precipitation of inorganic calcite under laboratory conditions. *Earth Planet. Sci. Lett.* **333–334**, 304–316.

Ling M.-X., Liu Y.-L., Williams I. S., Teng F.-Z., Yang X.-Y., Ding X., Wei G.-J., Xie L.-H., Deng W.-F. and Sun W.-D. (2013) Formation of the world's largest REE deposit through protracted fluxing of carbonatite by subduction-derived fluids. *Sci. Rep.* **3**, 1776.

Mackenzie F. T., Bischoff W. D., Bishop F. C., Loijens M., Schoonmaker J. and Wollast R. (1983) Magnesian calcites: Low-temperature occurrence, solubility and solid-solution behavior. *Rev. Mineral. Geochem.* **11**, 97–144.

Mavromatis V., Gautier Q., Bosc O. and Schott J. (2013) Kinetics of Mg partition and Mg stable isotope fractionation during its incorporation in calcite. *Geochim. Cosmochim. Acta* **114**, 188–203.

Mavromatis V., Pearce C. R., Shirokova L. S., Bundeleva I. A., Pokrovsky O. S., Benezeth P. and Oelkers E. H. (2012) Magnesium isotope fractionation during hydrous magnesium carbonate precipitation with and without cyanobacteria. *Geochim. Cosmochim. Acta* **76**, 161–174.

Mavromatis V., Immenhauser A., Buhl D., Purgstaller B., Baldermann A. and Dietzel M. (2017a) Effect of organic ligands on Mg partitioning and Mg isotope fractionation during low-temperature precipitation of calcite in the absence of growth rate effects. *Geochim. Cosmochim. Acta* **207**, 139–153.

Mavromatis V., Purgstaller B., Dietzel M., Buhl D., Immenhauser A. and Schott J. (2017b) Impact of amorphous precursor phases on magnesium isotope signatures of Mg-calcite. *Earth Planet. Sci. Lett.* **464**, 227–236.

Morse J. W. and Bender M. L. (1990) Partition coefficients in calcite: examination of factors influencing the validity of experimental results and their application to natural systems. *Chem. Geol.* **82**, 265–277.

Morse J. W., Wang Q. and Tsio M. Y. (1997) Influences of temperature and Mg: Ca ratio on $CaCO_3$ precipitates from seawater. *Geology* **25**, 85–87.

Mucci A. (1987) Influence of temperature on the composition of magnesian calcite overgrowths precipitated from seawater. *Geochim. Cosmochim. Acta* **51**, 1977–1984.

Mucci A. and Morse J. W. (1983) The incorporation of Mg^{2+} and Sr^{2+} into calcite overgrowths: influences of growth rate and solution composition. *Geochim. Cosmochim. Acta* **47**, 217–233.

Mucci A., Morse J. W. and Kaminsky M. S. (1985) Auger spectroscopy analysis of magnesian calcite overgrowths precipitated from seawater and solutions of similar composition. *Am. J. Sci.* **285**, 289–305.

Nielsen L. C., DePaolo D. J. and De Yoreo J. J. (2012) Self-consistent ion-by-ion growth model for kinetic isotopic fractionation during calcite precipitation. *Geochim. Cosmochim. Acta* **86**, 166–181.

Ning M., Huang K., Lang X., Ma H., Yuan H., Peng Y. and Shen B. (2019) Can crystal morphology indicate different generations of dolomites? Evidence from magnesium isotopes. *Chem. Geol.* **516**, 1–17.

Paquette J. and Reeder R. J. (1990) New type of compositional zoning in calcite: insights into crystal-growth mechanisms. *Geology* **18**, 1244.

Paquette J. and Reeder R. J. (1995) Relationship between surface structure, growth mechanism, and trace element incorporation in calcite. *Geochim. Cosmochim. Acta* **59**, 735–749.

Parkhurst D. L. and Appelo C. (2013) *Description of Input and Examples for PHREEQC Version 3: A Computer Program for Speciation, Batch-reaction, One-dimensional Transport, and Inverse Geochemical Calculations*. US Geological Survey.

Pearce C. R., Saldi G. D., Schott J. and Oelkers E. H. (2012) Isotopic fractionation during congruent dissolution, precipita-

tion and at equilibrium: evidence from Mg isotopes. *Geochim. Cosmochim. Acta* **92**, 170–183.

Pinilla C., Blanchard M., Balan E., Natarajan S. K., Vuilleumier R. and Mauri F. (2015) Equilibrium magnesium isotope fractionation between aqueous Mg^{2+} and carbonate minerals: Insights from path integral molecular dynamics. *Geochim. Cosmochim. Acta* **163**, 126–139.

Pogge von Strandmann P. A. E., Forshaw J. and Schmidt D. N. (2014) Modern and Cenozoic records of seawater magnesium from foraminiferal Mg isotopes. *Biogeosciences* **11**, 5155–5168.

Ra K., Kitagawa H. and Shiraiwa Y. (2010) Mg isotopes and Mg/Ca values of coccoliths from cultured specimens of the species Emiliania huxleyi and Gephyrocapsa oceanica. *Mar. Micropaleontol.* **77**, 119–124.

Reddy M. M. and Gaillard W. D. (1981) Kinetics of calcium carbonate (calcite)-seeded crystallization: Influence of solid/solution ratio on the reaction rate constant. *J. Colloid Interf. Sci.* **80**, 171–178.

Riechelmann S., Buhl D., Schröder-Ritzrau A., Riechelmann D. F. C., Richter D. K., Vonhof H. B., Wassenburg J. A., Geske A., Spötl C. and Immenhauser A. (2012) The magnesium isotope record of cave carbonate archives. *Clim. Past* **8**, 1849–1867.

Romanek C. S., Grossman E. L. and Morse J. W. (1992) Carbon isotopic fractionation in synthetic aragonite and calcite: effects of temperature and precipitation rate. *Geochim. Cosmochim. Acta* **56**, 419–430.

Rustad J. R., Casey W. H., Yin Q.-Z., Bylaska E. J., Felmy A. R., Bogatko S. A., Jackson V. E. and Dixon D. A. (2010) Isotopic fractionation of $Mg^{2+}_{(aq)}$, $Ca^{2+}_{(aq)}$, and $Fe^{2+}_{(aq)}$ with carbonate minerals. *Geochim. Cosmochim. Acta* **74**, 6301–6323.

Saenger C. and Wang Z. (2014) Magnesium isotope fractionation in biogenic and abiogenic carbonates: implications for paleoenvironmental proxies. *Quat. Sci. Rev.* **90**, 1–21.

Saulnier S., Rollion-Bard C., Vigier N. and Chaussidon M. (2012) Mg isotope fractionation during calcite precipitation: an experimental study. *Geochim. Cosmochim. Acta* **91**, 75–91.

Schauble E. A. (2011) First-principles estimates of equilibrium magnesium isotope fractionation in silicate, oxide, carbonate and hexaaquamagnesium (2+) crystals. *Geochim. Cosmochim. Acta* **75**, 844–869.

Schott J., Mavromatis V., Fujii T., Pearce C. R. and Oelkers E. H. (2016) The control of carbonate mineral Mg isotope composition by aqueous speciation: theoretical and experimental modeling. *Chem. Geol.* **445**, 120–134.

Schott J., Mavromatis V., González-González A. and Oelkers E. H. (2014) Kinetic and thermodynamic controls of divalent metals isotope composition in carbonate: experimental investigations and applications. *Procedia Earth and Planet. Sci.* **10**, 168–172.

Tang J., Dietzel M., Böhm F., Köhler S. J. and Eisenhauer A. (2008) Sr^{2+}/Ca^{2+} and $^{44}Ca/^{40}Ca$ fractionation during inorganic calcite formation: II. Ca isotopes. *Geochim. Cosmochim. Acta* **72**, 3733–3745.

Tang J., Niedermayr A., Köhler S. J., Böhm F., Kısakürek B., Eisenhauer A. and Dietzel M. (2012) Sr^{2+}/Ca^{2+} and $^{44}Ca/^{40}Ca$ fractionation during inorganic calcite formation: III. Impact of salinity/ionic strength. *Geochim. Cosmochim. Acta* **77**, 432–443.

Teng F.-Z. (2017) Magnesium Isotope Geochemistry. *Rev. Mineral. Geochem.* **82**, 219–287.

Teng F.-Z., Wadhwa M. and Helz R. T. (2007) Investigation of magnesium isotope fractionation during basalt differentiation: implications for a chondritic composition of the terrestrial mantle. *Earth Planet. Sci. Lett.* **261**, 84–92.

Teng F.-Z., Li W.-Y., Ke S., Yang W., Liu S.-A., Sedaghatpour F., Wang S.-J., Huang K.-J., Hu Y., Ling M.-X., Xiao Y., Liu X.-M., Li X.-W., Gu H.-O., Sio C. K., Wallace D. A., Su B.-X., Zhao L., Chamberlin J., Harrington M. and Brewer A. (2015) Magnesium isotopic compositions of international geological reference materials. *Geostand. Geoanal. Res.* **39**, 329–339.

Teng H. H., Dove P. M. and De Yoreo J. J. (1999) Reversed calcite morphologies induced by microscopic growth kinetics: insight into biomineralization. *Geochim. Cosmochim. Acta* **63**, 2507–2512.

Teng H. H., Dove P. M. and De Yoreo J. J. (2000) Kinetics of calcite growth: surface processes and relationships to macroscopic rate laws. *Geochim. Cosmochim. Acta* **64**, 2255–2266.

Wang W., Qin T., Zhou C., Huang S., Wu Z. and Huang F. (2017) Concentration effect on equilibrium fractionation of Mg-Ca isotopes in carbonate minerals: insights from first-principles calculations. *Geochim. Cosmochim. Acta* **208**, 185–197.

Wang W., Zhou C., Liu Y., Wu Z. and Huang F. (2019) Equilibrium Mg isotope fractionation among aqueous Mg^{2+}, carbonates, brucite and lizardite: insights from first-principles molecular dynamics simulations. *Geochim. Cosmochim. Acta* **250**, 117–129.

Wang Z., Hu P., Gaetani G., Liu C., Saenger C., Cohen A. and Hart S. (2013) Experimental calibration of Mg isotope fractionation between aragonite and seawater. *Geochim. Cosmochim. Acta* **102**, 113–123.

Wasylenki L. E., Dove P. M. and De Yoreo J. J. (2005) Effects of temperature and transport conditions on calcite growth in the presence of Mg^{2+}: implications for paleothermometry. *Geochim. Cosmochim. Acta* **69**, 4227–4236.

Watkins J. M., Nielsen L. C., Ryerson F. J. and DePaolo D. J. (2013) The influence of kinetics on the oxygen isotope composition of calcium carbonate. *Earth Planet. Sci. Lett.* **375**, 349–360.

Wombacher F., Eisenhauer A., Böhm F., Gussone N., Regenberg M., Dullo W. C. and Rüggeberg A. (2011) Magnesium stable isotope fractionation in marine biogenic calcite and aragonite. *Geochim. Cosmochim. Acta* **75**, 5797–5818.

Zuddas P. and Mucci A. (1994) Kinetics of calcite precipitation from seawater: I. A classical chemical kinetics description for strong electrolyte solutions. *Geochim. Cosmochim. Acta* **58**, 4353–4362.

Associate editor: Adrian Immenhauser